TURBOMACHINERY & PUMP SYMPOSIA | HOUSTON, TX
SEPTEMBER 13-15, 2022
SHORT COURSES: SEPTEMBER 12, 2022

AN IMPROVED THRUST PREDICTION MODEL FOR HIGH PRESSURE MULTI-STAGE CENTRIFUGAL COMPRESSORS

Anand Srinivasan
Senior Principal Engineer
Solar Turbines Inc.,
San Diego, California, USA

Edward J. Fowler
Senior Consulting Engineer
Solar Turbines Inc.,
San Diego, California, USA

Russell K. Marechale
Senior Consulting Engineer
Solar Turbines Inc.,
San Diego, California, USA

ABSTRACT

Axial thrust load predictions are an important aspect when it comes to predicting the performance of centrifugal compressors. The accurate prediction of axial thrust forces is necessary to size the appropriate balance piston and the thrust bearing dimensions for the operating limits of the compressor. Inline centrifugal compressors utilized for pipeline compression (and multistage upstream & midstream applications) often have a range of operating conditions, varying in flow, speed and discharge pressure (in addition to other variables such as gas composition and ambient conditions). The ability to accurately predict thrust loads over these ranges is thus important, especially at discharge pressures exceeding 3,000 psia [207 bar].

The key to predicting axial thrust forces lies in estimating the swirl ratio in the front and rear cavities of a shrouded impeller. This paper presents the modeling techniques for the prediction of swirl ratios in cavities as validated with scaled testing at the original equipment manufacturer's (OEM) facility. The extension of this proposed model for full-scale compressor models, along with test results on high pressure compressors operating at 4,285 psia [295 bar] has also been presented. The ability to validate thrust modeling procedures in the absence of load cell measurements from thrust bearings is detailed in this paper.

INTRODUCTION

The accurate determination of axial thrust loads is vital (Bidaut et al, 2014) for effective design of high pressure multi-stage centrifugal compressors. The thrust force on an impeller arises due to pressure imbalance between the front and rear faces of the impeller. The net axial thrust on the compressor rotor is a sum of the forces on each of the individual stages. The magnitudes of these forces are typically large on each face of a stage, and are compensated by appropriately sizing a balance piston diameter (or corresponding seal diameter) to counter the net thrust force. The axial thrust forces change as a function of speed and the operating point on the performance map. Accurate predictions for thrust forces are required to adequately size the thrust bearing.

A key aspect in understanding and quantifying thrust forces lies in the accurate calculations for leakage and swirl velocities at each impeller and the balance piston seal (Baldassarre et al, 2015). In the case of a shrouded impeller, the secondary leakage path for recirculation occurs on the eye and hub seals. The leakage rate is an important factor for determining the swirl ratio in the cavity, which is needed to calculate the static pressure distribution in the cavity. While the balance piston leakage can be measured, the measurement of shroud and hub seal leakages on industrial turbomachinery is often not feasible. Bulk-flow or CFD models (Kurz et al, 2011) are utilized for the leakage calculations at the individual impeller shroud and hub seals.

A measurement of the axial forces on the rotor is only feasible if load cells are installed in the thrust bearings. In the absence of load cells, the only practical measurement that is most often obtainable from an industrial centrifugal compressor is the thrust bearing

temperature. In this paper, the location of the thrust bearing is in the forward position (on the suction side of the compressor rotor). As the inlet flow to the compressor is throttled from the choke-side (high flow side) of the map to near surge, the net axial forces thrust the rotor towards the suction side of the impeller. This can be noted as an increase in the outboard thrust bearing temperatures. A thrust neutral point (i.e., the flow condition at which the net axial thrust on the rotor balances to zero) can occur in certain cases, where the thrust bearing temperatures equal on both the inboard and outboard pads. The measured thrust bearing temperatures can be used in combination with the predicted thrust loads by utilizing the thrust neutral point as a reference. In addition, the use of scaled single-stage rig testing with the use of CFD can also be implemented to ascertain the validity of the thrust predictions. The current work aims to present such a methodology for predicting thrust loads on multi-stage inline centrifugal compressors with shrouded impellers as validated by this OEM. It should be noted here that CFD predictions have a computational cost associated with it (especially in the case of multistage compressors), and hence the need for a bulk-flow prediction is vital for performance predictions.

The remainder of this paper is arranged as follows; we start with an overview of axial thrust loads in centrifugal compressors and the methodology for predictions. The next section covers the overview of the results obtained from the test rig, which was used to update the OEM's thrust prediction models. An application of the updated model was validated with CFD predictions on a single stage pipeline compressor design. Finally, test data was obtained from a multi-stage centrifugal compressor at discharge pressures up to 4,285 psia [295 bar] and serves as a validation for the predicted versus measured thrust neutral flow point.

THRUST MODEL

The axial thrust forces on a stage of centrifugal compression occurs due to the differential pressure between the front and rear faces of the impeller. In the case of a shrouded impeller, the differential pressure generated at the front and rear cavities (and at the hub) account for the pressure forces on the impeller. In addition to the pressure forces, the change of momentum in the impeller is a result of the axial velocity component at the inlet, and this accounts for the momentum forces. This is a direct result of the difference in velocity between the inlet and exit of the impeller and is a function of the density of the gas and the rotational speed. The net force on the impeller can be represented as

$$F_{impeller} = F_{pressure} + F_{momentum} \tag{1}$$

The axial forces generated by the impeller are balanced by labyrinth (or other) seals at the balance piston or hub locations, where the diameter is carefully chosen to attempt to negate the effects of the pressure and momentum forces on the impeller.

$$F_{net} = F_{impeller} + F_{seal} \tag{2}$$

Several challenges arise in the accurate evaluation of the thrust forces (Bidaut et al, 2016). While it is possible to choose a seal diameter to offset the net forces to equate to zero in theory, achieving this in practice is nearly impossible. The pressure forces on the impeller are clearly related to the suction and discharge conditions of the compressor. As a result, changes in operating conditions even at a fixed speed (as the flow shifts across the map) results in changes to the pressure forces (Kurz et al, 2011). Moreover, changes in speed can result in changes to the momentum forces. As a result, the net force on the impeller is seldom constant (nor is it possible to achieve zero net-forces across all operating conditions). The thrust bearings are intended to help handle the axial loads that remain after having been balanced out by the balance piston seal. Hence, it is important to accurately predict the range of axial thrust forces that the thrust bearing ought to accommodate over the operating conditions of the compressor.

A second challenge that arises with thrust predictions is with multi-stage compression, where the vector-summation of forces of large magnitudes are effectively handled by adjusting the balance piston diameter. The axial thrust on the compressor rotor is the net total of the pressure and momentum forces generated on each stage of compression. Table 1 shows the predicted thrust forces on a six-stage centrifugal compressor with shrouded impellers. The predictions were performed with natural gas as the medium operating at 14,000 rpm. The suction and discharge conditions are 1,500 psia [103 bar] and 4,100 psia [282 bar]. It can be observed that the pressure forces on the front and rear of each stage of compression is (on average) an order of magnitude higher than the net force on each stage. Uncertainties in the predictions for these forces of large magnitude can lead to large variations in the net axial thrust generated by the rotor. The need for accurate stage-by-stage predictions that depend on the shroud (and hub) seal leakages (and swirl ratios) is underscored by this example.

The influence of the balance piston seal diameter in handling the thrust generated by the impellers is also illustrated in table 1. Modifying the balance piston diameter from 7.9 in [200.6 mm] to 8.1 in [205.7 mm] results in the net balance piston force to change by approximately 5,600 lbf [24,910 N] in this case, resulting in the net axial thrust on the rotor to change from 5,317 lbf [23,651 N] to -599 lbf [-2,664 N]. While it appears that the magnitude of the thrust force has been reduced by modifying the balance piston diameter, this illustrative example is valid at the specified flow condition. Changes to speed, suction pressure and flow conditions can result in a range of thrust loads generated by the impellers, and a nominal balance piston diameter is often selected to minimize the net axial force. This remaining axial thrust force is then handled by the thrust bearings.

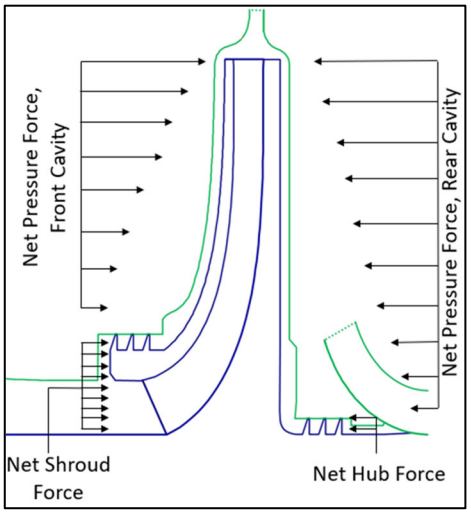

Stage	Hub + Shroud Force		Net Pressure Force		Momentum Force		Net Impeller Force Per Stage	
	[lb]	[N]	[lb]	[N]	[lb]	[N]	[lb]	[N]
1	40746	181320	35504	157993	328	1460	4914	21867
2	48890	217561	42966	191199	294	1308	5630	25054
3	53670	238832	47458	211188	286	1273	5926	26371
4	60340	268513	53638	238689	272	1210	6430	28614
5	64891	288765	57828	257335	269	1197	6794	30233
6	65868	293113	58640	260948	280	1246	6948	30919

	Net Force	
	[lb]	[N]
Net Impeller Thrust	36642	163057
Resultant Balance Piston Force, 7.9" dia	-31332	-139427
Resultant Balance Piston Force, 8.1" dia	-37241	-165722
Net Axial Thrust, 7.9" dia	5317	23661
Net Axial Thrust, 8.1" dia	-599	-2666

Table 1. Thrust forces of the impeller; positive forces are towards the suction end

The parasitic losses in the front and rear cavities are a function of the leakage, windage and disk friction and are therefore dependent on the clearance gap at the shroud seals. The pressure drop across the cavity as a function of radius is given by

$$\frac{\partial P}{\partial r} = K^2 \omega^2 \rho r \tag{3}$$

The significance of the above equation (where other insignificant terms have been dropped out for brevity) is that the pressure drop along a cavity can be determined using the pressure at the tip of the impeller and scaled as a function of radius. This helps in defining the static pressure at the upstream of the first tooth of the shroud seal, and thus enables the calculation of the seal leakage. The accuracy of the calculation depends heavily on the constant K, which is the swirl ratio. The assumption of a constant swirl ratio with values chosen from empirical or historical estimates holds good for low pressure applications. However, its applicability over a range of flows and Reynolds numbers may not be valid. We provide further details in this regard in the following sections of the paper.

Aungier (2000) notes that the swirl ratio is a function of the leakage and determined using

$$\mathrm{K} = \mathrm{K_0} + \mathrm{C_q}\left(1.75\frac{\mathrm{C_{U2}}}{\mathrm{U_2}} - 0.316\right)\frac{r_2}{s} \tag{4}$$

where s is the axial gap (between the impeller and stator cavity) and r_2 the impeller outer radius, and

$$C_q = \frac{\dot{m}\left(\frac{\rho r_2 U_2}{\mu}\right)^{(1/5)}}{2\pi\rho r_2^2 U_2} \tag{5}$$

and

$$K_0 = \frac{0.46}{1 + \frac{s}{r_2}} \tag{6}$$

A cursory glance at eqns. (4)-(6) reveals that the swirl ratio is a function of the leakage across the shroud and hub seals, which in turn is a function of the differential pressure across the seal. Hence, an iterative approach is necessary to calculate the swirl ratio and the differential pressure across the seal. These equations also highlight the need for a non-constant swirl ratio across flow ranges at different operating conditions. As the inlet flow to the compressor is throttled towards surge, the leakage rate increases (due to the increase in discharge pressure), and thus the swirl ratio also changes.

The above model does not include the effect of disk friction as a function of Reynolds number. Daily & Nece (1960) provide criteria for calculating the disk friction coefficient for laminar and turbulent flow regimes with merged and separated boundary layers. Based on the specific regime for the flow condition, the multiplier for the C_q coefficient, C_m^* is calculated. For the cases with through-flow and

zero pre-swirl, the swirl ratio is calculated as suggested by Daily & Nece, as follows:

$$K = \frac{K_0}{C_m^* C_q + 1} \tag{7}$$

The empirical form of the swirl ratio calculation as implemented by this OEM for non-zero pre-swirl was determined to be

$$K_{0adj} = 1 - \alpha\left(1 - \frac{C_{U2}}{U_2}\right)^{\beta} \tag{8}$$

and

$$K = K_{0adj} + \frac{K_0 - K_{0adj}}{\gamma C_q + 1} \tag{9}$$

The coefficients $C_m^*, \alpha, \beta, \gamma$ were determined empirically from the results of the scaled testing, as outlined in the following section. As a result of Daily & Nece's criteria for flow regimes with adjustment for fully rough flow, the applicability of this model can be extended to Reynolds numbers ranging from laminar to fully turbulent and for smooth to fully rough flow regimes. The results reported in this paper have been validated for Reynolds numbers ranging from ~2.0E6 partly rough to ~2.0E8 fully rough flow regimes, all cases being turbulent with separate boundary layers.

SCALED TESTING

Testing was conducted on a scaled rig at the OEM's facility with air as the test medium. The test setup comprised of an inlet guide vane (IGV) with a single-stage impeller, followed by a return vane. A cross-section view of the test setup is shown in fig. (1). The rotor was driven by a motor coupled via a gearbox. The front shroud was instrumented with static pressure tap measurements at four radial locations (fig. (1), right). The measurements from these static pressure taps were utilized to obtain the swirl ratios for the front cavity. Testing was performed at 13,100 rpm on air at 80 psia [5.5 bar] suction pressure. Both the hub and shroud seals used in this test rig were babbitted type, with clearances set at nominal (0.003 in [0.076 mm] radial, denoted as 1X seal clearance) and 4-times the nominal (denoted as 4x seal clearance). Figure (2) shows the as-tested results for the pressure profiles and the swirl ratios from the scaled test rig. Also plotted in fig. (2) are the swirl ratios on the front cavity based on a CFD prediction of the scaled test rig. In addition, the updated swirl model with the coefficients in eq. (9) that were tuned to match the test results are also shown. In addition to the results noted in fig. (2), further in-house validations of the proposed model were performed with testing at different machine Mach numbers, impellers with different specific speeds and with shroud seal clearances that were varied from the numbers noted in fig. (2). The proposed model for the swirl ratios was observed to follow the as-tested data in all cases. The updated model was then implemented as part of the OEM's

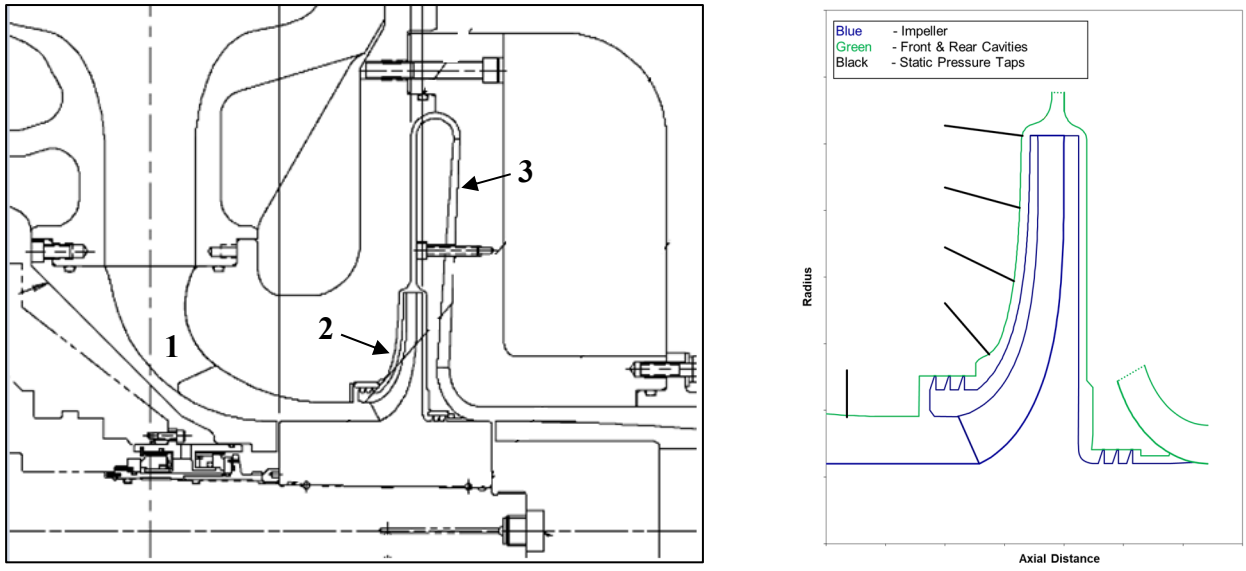

Figure 1. Cross section of the scaled test rig (left) and locations of static pressure taps along the front shroud (right); Labeled sections: 1 = inlet guide vane, 2 = impeller with front and rear shrouds, 3 = return vane

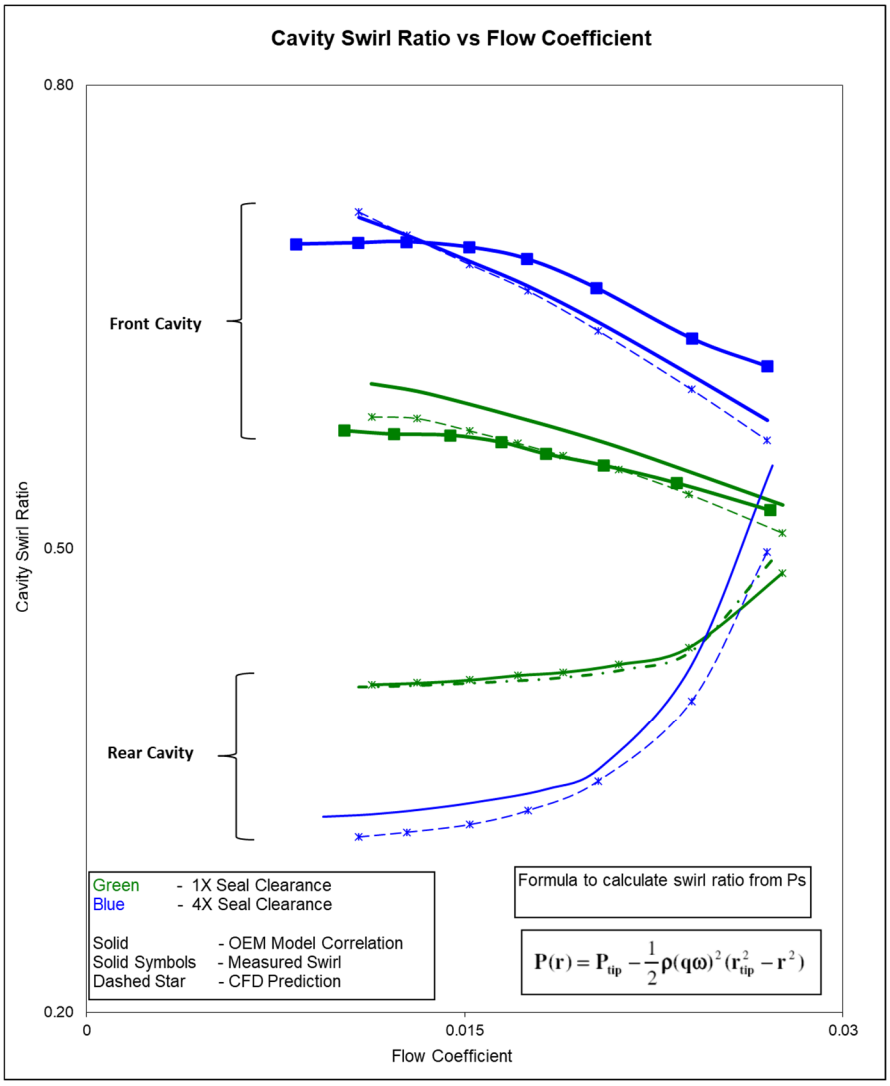

Figure 2. Cavity tests for increasing flows and two seal clearances obtained from the scaled test rig

in-house aerodynamic performance calculation software for thrust load predictions. The extension of this updated model from the scaled test rig to predicting thrust loads on full-scale compressors is outlined in the following sections.

VALIDATION WITH CFD FOR PIPELINE COMPRESSOR STAGE

The updated bulk flow prediction for thrust loads outlined in the previous section was compared with CFD predictions, and the results are summarized in this section. A pipeline compressor stage was considered for the purpose of this study. The simulations were performed in CFD with air as the medium at 14.7 psia [1 bar] suction pressure and 8,000 rpm. The 15-bladed impeller was modeled as a pie-slice in CFD (using Ansys CFX) and a steady-state analysis was performed. The SST-turbulence model was implemented with pressure & temperature as the inlet, and mass flow as the exit boundary conditions. The impeller and cavity meshes were comprised of 737,000 & 835,000 nodes respectively. Convergence was guaranteed by ensuring that the Y+ values for the rotating domains in the CFD setup remained below 5.0. The two configurations that were analyzed are summarized below:

- Configuration #1 – impeller domain with a balance piston on the rear cavity, and a vertical diffuser at the exit.
- Configuration #2 – impeller domain with a hub seal on the rear cavity, and a return vane at the exit.

A schematic of the CFD setup is shown in fig. (3).

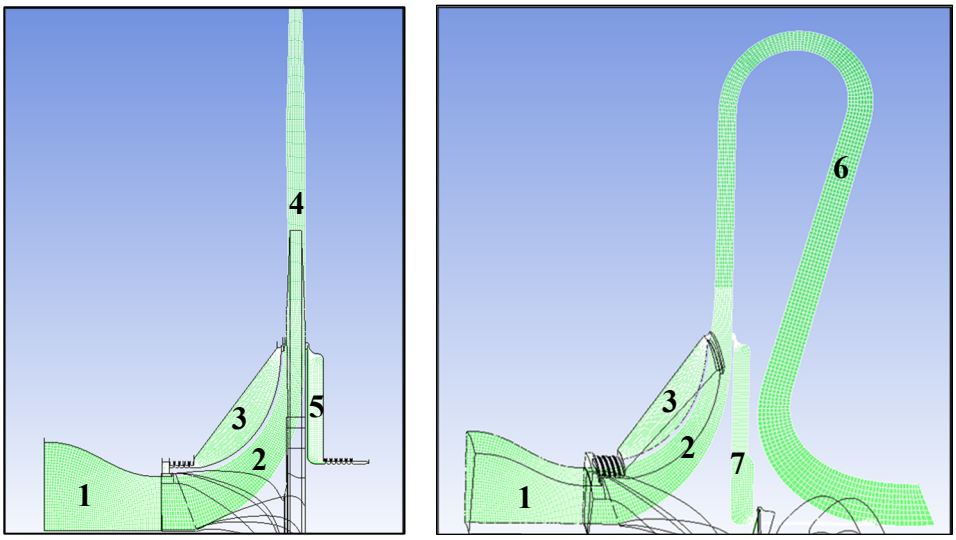

Figure 3. Cross-section of the CFD setup, Configuration #1 (left), Configuration #2 (right); Labeled domains: 1 = inlet duct, 2 = impeller, 3 = front cavity, 4 = exit diffuser, 5 = balance piston, 6 = return vane, 7 = rear cavity

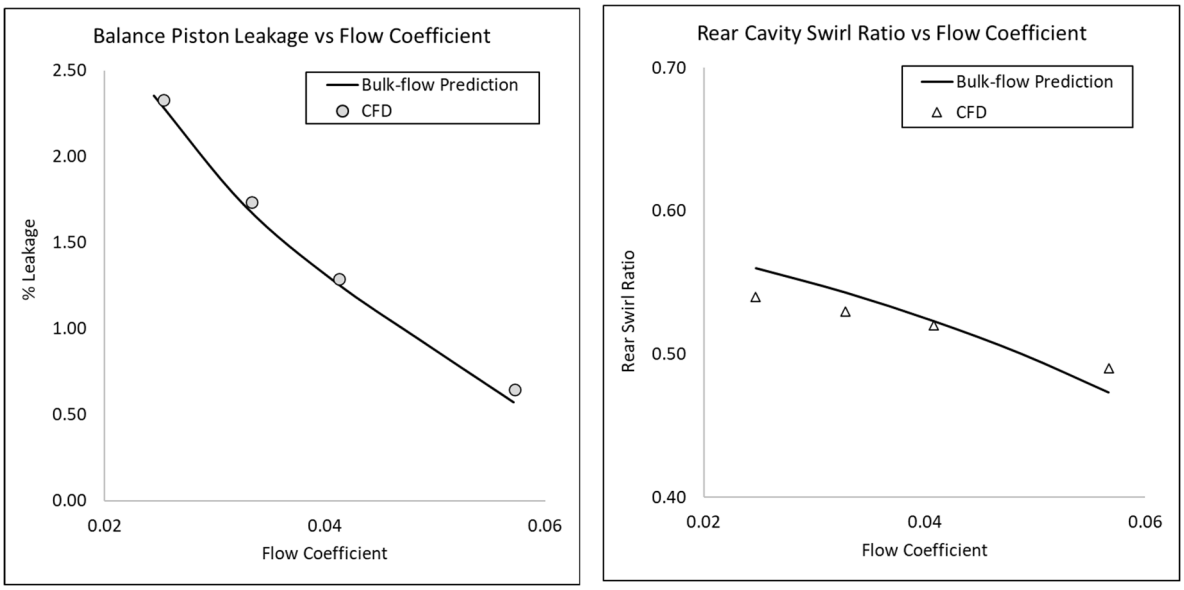

Figure 4. Balance piston leakage (left) and rear cavity swirl ratio (right), CFD vs bulk-flow prediction

In each configuration, pressure-boundary conditions were used at the inlet, and mass flow was specified at the exit. A pressure-boundary condition was also enforced on the outboard side of the balance piston for configuration #1. Both configurations included a secondary leakage path via the front shroud (in addition to the rear shroud). The leakage rates from the secondary flow paths on both the front and rear cavities were computed from CFD and compared against the bulk flow model. The swirl ratio at each flow condition was calculated by post-processing the static pressure profiles as obtained from CFD and fitting it to match the integrated from of eq. (3). The swirl ratios were then compared with the updated model described in the prior section. Figure (4) shows the leakage rate and the swirl ratio comparison between the bulk flow model prediction & CFD, for the balance piston and the rear cavity. Figure (5) shows the same comparison for the secondary leakage path of the front shroud.

It can be noted from fig. (4, 5) that the updated swirl model matches qualitatively well with the CFD predictions. More importantly, the predictions further validate the need for the improved thrust model with non-constant swirl ratios over a range of operating conditions. It can be observed from fig. (5) that the swirl ratio at flow point B (the best efficiency point) as predicted by CFD matches well with that of the bulk-flow model's prediction. However, the flow point A (the surge flow point) shows that the predicted swirl from CFD falls below that of the bulk-flow prediction. This can be further explained in the static pressure profiles as a function of radius as noted in fig. (6). Here, the static pressure profiles have been plotted along the front cavity as a function of the radius normalized to the impeller

tip. The static pressures from CFD were also utilized to calculate a pressure distribution using eq. (3) for a specified swirl ratio. It can be noted that the specified swirl ratio for flow point B results in a static pressure profile that matches well with that of CFD. The variation in the static pressure profiles at flow point A for two different values of swirl ratios is observed to be minimal as shown in fig. (6). In summary, the proposed bulk-flow model for swirl ratios that was obtained using the scaled rig results match well with the CFD predictions when applied to a pipeline compressor stage.

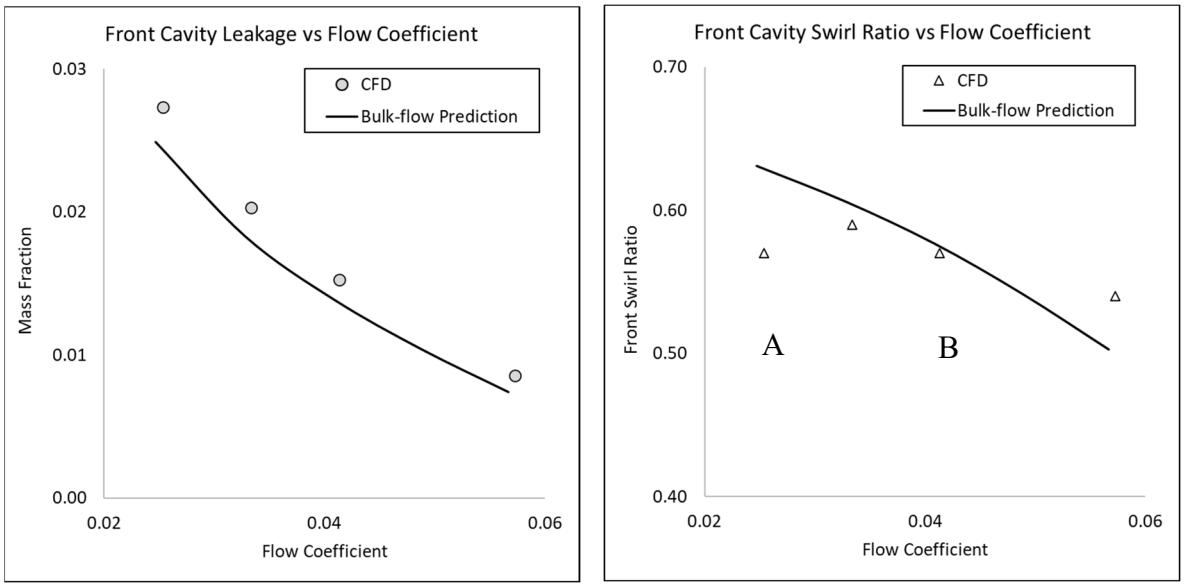

Figure 5. Front cavity leakage (left) and front cavity swirl ratio (right), CFD vs bulk flow prediction

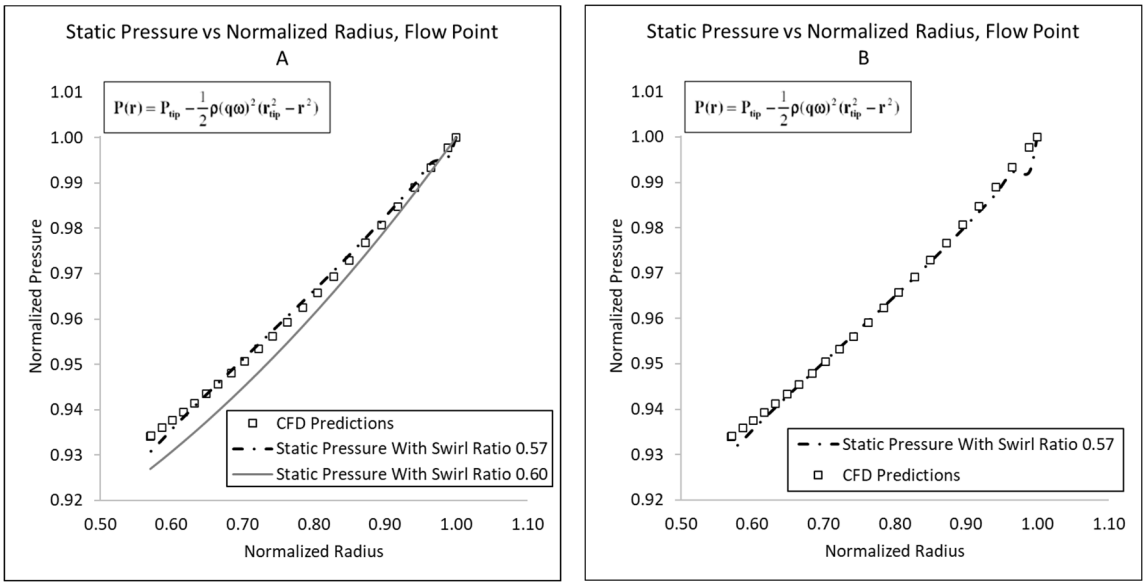

Figure 6. Static pressure vs radius normalized to impeller tip, flow points A (left) and B (right)

HIGH PRESSURE TESTING

In this section, we discuss the results obtained during in-house development testing of a gas compressor and the use of the tested results in validating the updated thrust model. Testing was performed at the OEM's closed loop facility. The subject inline centrifugal gas compressor was a six-stage design, with a high temperature babbitt balance piston seal. The compressor was driven by a gas turbine coupled through a gearbox.

Figure 7a. Closed-loop arrangement of the high pressure compressor

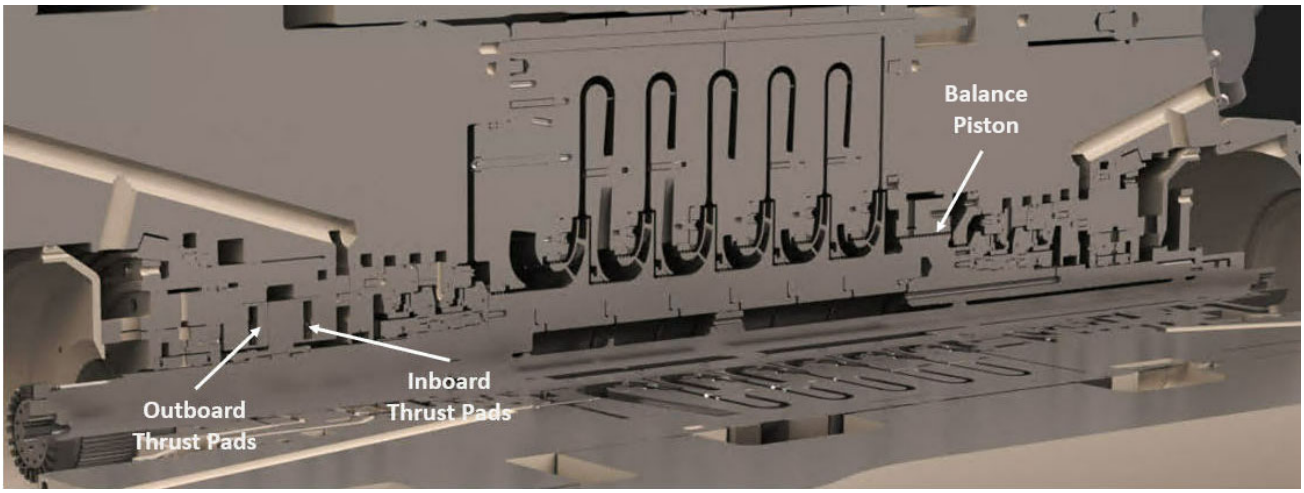

Figure 7b. Cross-section of the test compressor

Testing was performed with nitrogen and natural gas as part of the aerodynamic performance evaluation. The compressor was operated at a fixed speed starting at the highest flow condition, with multiple flow points taken as the flow was throttled to near surge. The compressor was allowed to attain steady state at each flow point to ensure thermal equilibrium before data was collected. Testing on nitrogen was performed at 12,700 rpm (aerodynamic Machine Mach number of 0.54) with a suction pressure held constant at 1,200 psia [82.7 bar]. The highest discharge pressure attained near surge was 3,670 psia [253 bar]. Testing on natural gas was performed at 14,000 rpm (Machine Mach number of 0.50), with suction pressure held at 1,580 psia [109 bar]. The highest discharge pressure attained in this case was 4,285 psia [295 bar].

The thrust bearings were of tilting-pad type, with temperature probes embedded on two pads (bottom and top) of the inboard and outboard halves. The temperatures were recorded as a time-averaged measurement of 60 samples of data for each data point. Three such data points were recorded, and the averaged measurements (of the top and bottom pads) are reported in this section. The thrust bearing temperatures that were recorded during the performance evaluation are shown in fig. (8) as a function of the inlet flow coefficient. It can be observed from the plots that at high flows, the inboard thrust bearing is more heavily loaded and thus exhibits a higher temperature (compared to the outboard thrust bearing). As the flow is throttled towards surge, the temperatures cross-over and the outboard thrust bearing starts to get more heavily loaded. This indicates an axial movement of the rotor in a direction that is towards the outboard thrust bearing as the flow condition is throttled towards surge.

The flow condition at which the thrust bearing temperatures equal each other on the inboard and outboard faces is referred to as the thrust-neutral flow point. Also shown in fig. (8) are the predicted thrust-neutral flow point indicated by the vertical red lines. The dotted-red line shows the predicted thrust-neutral flow as obtained using the OEM's prior model with a constant swirl ratio assumption across the entire flow range. In contrast, the updated model (represented here by the solid red vertical line) shows a thrust-neutral flow point that more closely matches the measured thrust bearing temperature cross-over condition on both nitrogen and natural gas.

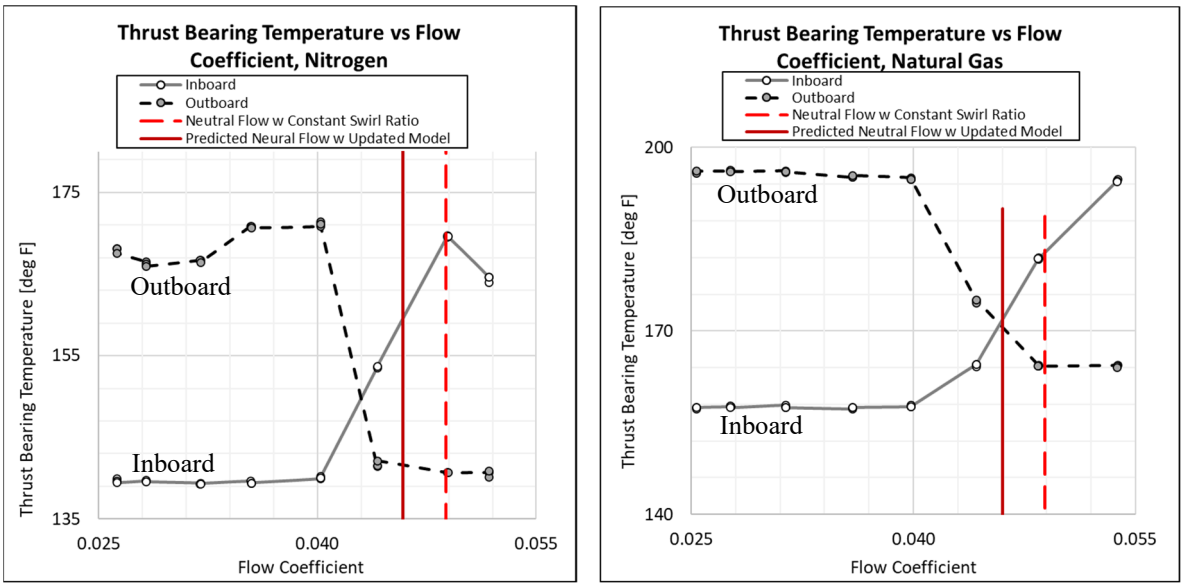

Figure 8. Thrust bearing temperatures vs flow coefficient with test gases nitrogen (left) and natural gas (right)

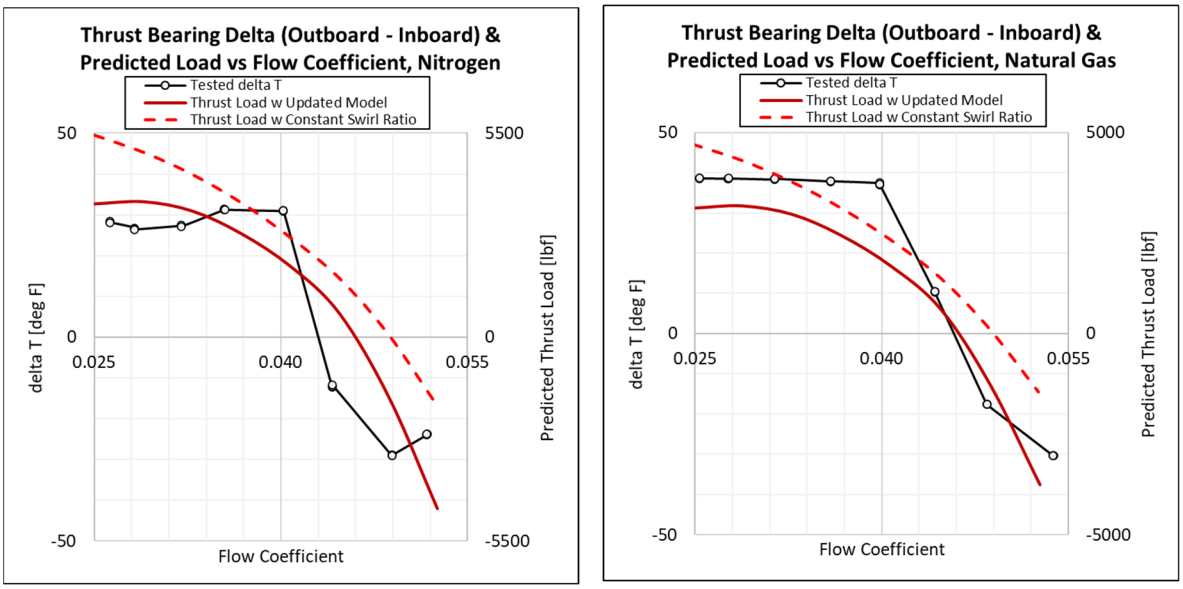

Figure 9. Thrust bearing differential temperature and predicted thrust load with test gases nitrogen (left) and natural gas (right)

The as-tested gas compressor lacked the instrumentation provisions for load cells on the thrust bearings. However, the predicted thrust loads can be compared with the measured thrust bearing temperatures to discern the differences between the two models. Figure (9) shows the thrust bearing temperatures (on the left-vertical axis), along with the predicted thrust loads (on the right-vertical axis). The as-measured thrust bearing temperatures were observed to exhibit a "flattening" of the temperatures at flow coefficient below 0.040. The as-predicted thrust load obtained using the updated OEM model also shows the load to flatten out at flow coefficient below 0.040. The prior model with the constant swirl ratio assumption does not exhibit any such flattening of the thrust load, and tends to predict an increasing load as flow is throttled towards surge. In summary, the updated thrust model qualitatively matches the as-tested thrust

bearing temperatures both in terms of predicting the thrust-neutral flow and the flattening of the temperatures near surge.

CONCLUSIONS

An overview of thrust load predictions for inline centrifugal compressors with shrouded impellers is presented in this paper. The proposed models for swirl ratio estimations are validated with results from a scaled test rig and with CFD predictions. The updated thrust prediction model is applied to a high pressure centrifugal compressor operating up to 4,285 psia [295 bar] discharge pressure, and the tested thrust bearing temperatures are reported. The steps followed in the validation of a thrust prediction methodology in the absence of actual load cell measurements from a thrust bearing are presented. The updated model for thrust prediction was observed to be an improvement when compared to prior thrust predictions as applied by this OEM. The updated model allows for a more accurate balance piston diameter sizing for multistage high pressure compressors.

NOMENCLATURE

r	= radius (L)
$F_{[\ ]}$	= force (subscript denotes component) (MLT^{-2})
K	= swirl ratio $\frac{C_{U2}}{U_2}$ (-)
ω	= speed (T^{-1})
ρ	= density (ML^{-3})
U_1, U_2	= inlet, tip velocity (MT^{-1})
$\dot{m}$	= mass flow (MT^{-1})
ϕ	= inlet flow coefficient $\frac{Q}{ND_2^3}$ (-)
Re	= Reynolds number $\frac{\rho r_2 U_2}{\mu}$ (-)
$C_m^*, \alpha, \beta, \gamma$	= empirical coefficients (-)

REFERENCES

Baldassarre, L., Fontana M., Bernocchi A., Maiuolo F., Rizzo E., 2015, Axial Thrust in High Pressure Centrifugal Compressors: Description of a Calculation Model Validated by Experimental Data from Full Load Test, Proceedings of the 44th Turbomachinery Symposium, Turbomachinery Laboratory, Texas A&M University, College Station, TX, https://doi.org/10.21423/R1HP7G.

Bidaut Y., Dessibourg D., 2014, The Challenge for the Accurate Determination of the Axial Rotor Thrust in Centrifugal Compressors, Proceedings of the 43rd Turbomachinery Symposium, Turbomachinery Laboratory, Texas A&M University, College Station, TX, https://doi.org/10.21423/R1QD7K.

Kurz R., Marechale R., Fowler E., Ji M., Cave M., 2011, Operation of Centrifugal Compressors in Choke Conditions, Proceedings of the 40th Turbomachinery Symposium, Turbomachinery Laboratory, Texas A&M University, College Station, TX, https://doi.org/10.21423/R16D89.

Aungier R., 2000, Centrifugal Compressors: A Strategy for Aerodynamic Design and Analysis, ASME Press.

Daily, J.W., Nece, R.E., 1960, Chamber Dimension Effects on Induced Flow and Frictional Resistance of Enclosed Rotating Disks, *Transactions ASME, Journal of Basic Engineering*, Mar., 217-232.

Japikse, David, 1996, *Centrifugal Compressor Design and Performance,* Concepts ETI, Inc., Wilder, VT.

Daily, J. W. and Nece, R. E., 1960, "Roughness Effects on Frictional Resistance of Enclosed Rotating Disks." *Transactions ASME, Journal of Basic Engineering*, Sept., 553-562.

ACKNOWLEDGEMENTS

The authors would like to thank Solar Turbines Inc. for their permission to present this paper.